Modeling and Simulation of a Novel Tilt-Wing-Coaxial-Rotor Tricopter

Alvaro D. H. Arroyo *. Aniel S. Morais.**
Gabriela V. Lima* Laura Ribeiro******

**Department of Electrical Engineering, Federal University of Uberlândia, Uberlândia, MG 38.408-100 Brazil (e-mail: alvaro.daniel@ufu.br, avalonskull_adha@hotmail.com)*
*** Department of Electrical Engineering, Federal University of Uberlândia, Uberlândia, Brazil (e-mail: aniel@ufu.br)*
****Department of Electrical Engineering, Federal University of Uberlândia, Uberlândia, Brazil (e-mail: gabriela.lima@ufu.br)*
*****Department of Electrical Engineering, Federal University of Uberlândia, Uberlândia, Brazil (e-mail: laurar@ufu.br)*

Abstract: The following paper presents the methodology proposed to describe the equations which may define the flight dynamics of a new tilt-wing-coaxial-rotor tricopter, with the ability to rotate independently its three coaxial rotors. To assertively describe the mechanics involved in such aircraft, forces and torques related to aerodynamical, propulsive and inertial principles are considered. Specially highlighting the non-linear attitude of the aircraft and its moving center of gravity (CG) due to its capability to assume a non-symmetrical morphology airborne. The non-linear mathematical model is essential to fully understand the behavior of a multi-body, omnidirectional, unmanned aerial vehicle (UAV) in order to apply control techniques to it. The inertial matrix that describes the mass distribution of the multi-body system, as function of the coaxial-rotors' tilt angles, is compared to the 3D model obtained in a computer-aided-design (CAD) software such as SolidWorks. Finally, a simulation using Linear Quadratic Regulation (LQR) control for a cruise (leveled flight) condition is analyzed in order to validate the dynamic behavior of the aircraft.

Keywords: Aerial robotics, Coaxial-rotor; Flight mechanics; Non-linear model; Simulation and control; Tilt-rotor; Tilt-wing; Tricopter.

1. INTRODUCTION

Over the last decade, with the ongoing development of Drones or UAVs, a wide variety of models have been tested and created, leading to especially two types of Drones: multi-copters and fixed-wings. Yet, recently, there has been an increasing demand to explore the "mixture" between these two types of drones, leading to Vertical-Take-Off-and-Landing drones (VTOL), which seek to produce an aircraft that is able to have the stability characteristics of a multi-copter in hover mode, and the speed and elevated flight time that a fixed-wing usually provides in cruise mode. Thus, VTOLs are capable of taking-off vertically, hover in the air, fly horizontally (by generating lift on its wings) and then land vertically. Unfortunately, this comes with the cost of complexity, by increasing significantly the non-linear degree of the system's dynamics.

Within the realm of VTOLs, several authors have been studying and testing different types of drone designs. As an example, Onen et al. (2015) proposes a conventional fixed-wing airplane with a tricopter architecture, in which the frontal rotors have the ability to rotate from their vertical position (helping lift the drone during take-off or landing) into a horizontal position when the drone starts the cruise mode, or horizontal flight. A similar model is studied by Bautista et al. (2017) in which a flying-wing is coupled with three tilting rotors. Another good example is Mikami et al. (2015) where the authors consider a double-winged aircraft (one at the front and one at the rear) where each wing has a couple of rotors mounted at the middle of their semi-spans. These wings rotate simultaneously when the drone transitions from a hover mode into cruise mode. On all these three cases, once the aircraft reaches the cruise mode, they use classical flight control surfaces such as ailerons, flaps, rudder or elevator in order to contribute to the control of the aircraft, as an airplane would. The review of Zhong et al. (2016) shows several VTOL models, which are characterized by their ability to rotate either just their rotors (classified by the authors as Tilt-rotor UAVs) or their rotors along with their wings (classified as Tilt-wing UAVs). In every model reviewed by the authors, classical flight control surfaces also seem to be used to contribute in the aircraft's control. Autenrieb et al. (2019) presents the control of a Tilt-wing aircraft with rotors at the tips of the wing and classical flight control surfaces to control it.

When using a rotor in an aircraft, it is necessary to consider the rotor's induced torque on the body or base where it is mounted, due to Newton's third law caused by the interaction of the air-flow passing through the propellers. Thus, every aircraft that uses rotors must use a mechanism to ensure the balance or cancellation of this induced torque and thus to control the attitude of the aircraft. In the case of a helicopter, for example, a rear rotor compensates for this torque while also providing yaw control. Another option to achieve this purpose is by using coaxial-rotors that can balance the induced torque (by rotating

its propellers in opposite directions), while also offer a greater thrust force than a single rotor would as shown by Alexis et al. (2013). The use of coaxial-rotors is well described by Allenspach et al. (2020) which is a crucial component to allow their Tilt-rotor hexacopter achieve an omnidirectional movement in the air.

The main goal of this research is to explore the dynamics of a new drone architecture with tilting-wings and coaxial-rotors in a tricopter configuration. The aircraft model proposed in this work has a coaxial-rotor mounted on the tip of each of its tilting-wings (with no ailerons or flaps), while also having a rear tilting-coaxial-rotor. Each wing is conceived with an independent rotation from each other, allowing the vectorization of the rotors' thrust forces and the wings' lift and drag forces as method to provide control and maneuverability while flying or hovering. An extensive research over renowned journals, including IEEE, shows that this drone architecture may be pioneer.

As will be explained in the following sections, the model's forces and torques related to aerodynamical, propulsive and inertial principles are considered. Highlighting that the inertial matrix could be non-symmetrical, as it is a function of the tilting angles.

2. DRONE DESCRIPTION

The aircraft is composed of three rigid bodies that spin around its fuselage *F* (considered the main body). The right wing W_1 plus the right coaxial-rotor R_1, mounted at its tip, represents the first set or rigid body rotating around the fuselage. The left wing W_2, plus its left coaxial-rotor R_2 (also at the tip), compose the second spinning set. Both wings rotate independently of each other around the fuselage in a "medium-wing" configuration, on a rotation axis close to the aircraft's nose. The third rigid body, with also independent rotation along the aircraft's longitudinal axis, is the rear coaxial-rotor R_3. A conceptual design of the drone in its hover and forward flight modes is presented in Fig. 1, from different perspectives.

Each wing is considered rectangular, with no torsion angle and with a symmetrical aerodynamic profile. The fuselage is designed based on the aerodynamic profile of the wing itself, in order to diminish drag forces over it.

Since the three rigid bodies of the aircraft rotate independently of each other around an axis that crosses the aircraft's fuselage, it is important to note that with each rotation of these components the CG of the aircraft will change its position in space. This is taken into account in the equation of inertia and active moments in the aircraft. The rotation of each wing and the rear coaxial-rotor is measured by their respective tilting angles ϕ_{Ei}, with i = 1, 2, 3 (for the wings, this also represent the incidence angles) and shown in Fig. 2. The tilting angles are considered to be at 0º when a given coaxial-rotor (lateral or rear) is horizontal and at 90º when is vertical and the thrust vector is pointing upwards.

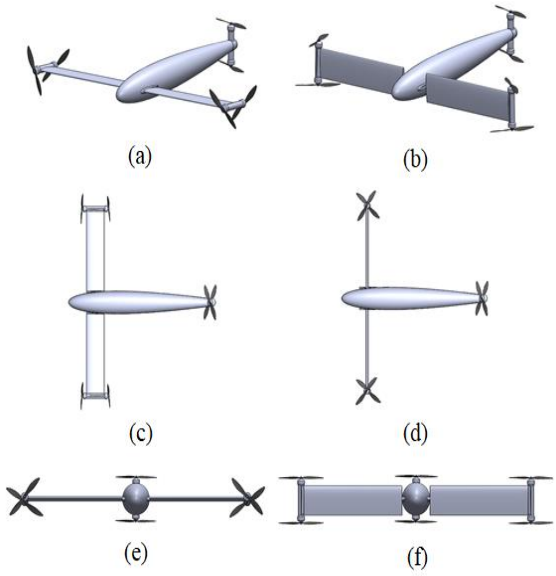

Fig. 1. Perspectives of the aircraft: (a) Forward flight in perspective, (b) Hover mode in perspective, (c) Upper view of forward flight, (d) Upper view of hover mode, (e) Front view of forward flight, (f) Front view of hover mode.

If both wings are not aligned with each other (i.e. $\phi_{E1} \neq \phi_{E2}$) or if the real coaxial-rotor is not pointing at 90º, then the aircraft will assume a non-symmetrical morphology, which implies that the products and moments of inertia must be considered at every moment as a function of the tilting angles.

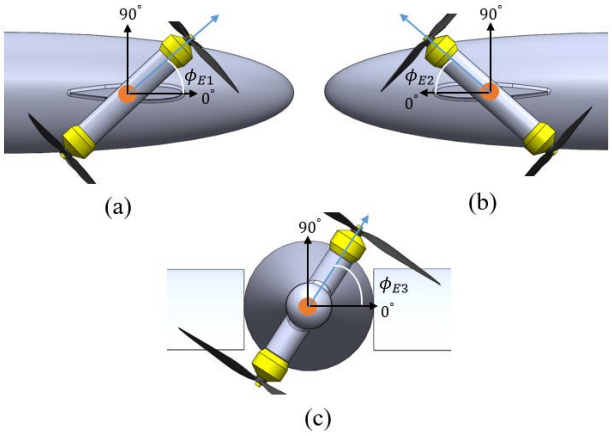

Fig. 2. Rotation of the tilting angles: (a) Right Wing-Coaxial-Rotor tilting angle ϕ_{E1}, (b) Left Wing-Coaxial-Rotor tilting angle ϕ_{E2}, (c) Rear Coaxial-Rotor tilting angle ϕ_{E3}.

3. REFERENCE SYSTEMS

The reference systems used is this model follow the right-hand rule and are described as the following:

Main Reference Systems

Inertial: *I*

- Attached to Earth's reference system;

- Axes $[X,Y,Z]_I$ oriented, respectively, towards North, East and towards Earth's core;

Body-fixed: *B*

- Origin at the aircraft's movable CG;
- Axes $[X,Y,Z]_B$ oriented, respectively, towards the aircraft's nose, right wing and aircraft's belly;
- Does spin with the aircraft.

Nose-fixed: *A*

- Origin fixed to the aircraft's nose;
- Axes $[X,Y,Z]_A$ always parallel to $[X,Y,Z]_B$;
- Does spin with the aircraft;
- Serves as a reference system to determine the aircraft's CG position.

Secondary Reference Systems

Parallel to body system *B*: *Pb*

- Origin at the CG of each component (wings, coaxial-rotors and fuselage);
- Axes $[X,Y,Z]_{Pb}$ always parallel to $[X,Y,Z]_B$;

The movable position of the aircraft's CG (and its fixed system *B*) is a function of the position of the center of gravity of each component (wings, coaxial-rotors and fuselage) relative to a fixed point in the aircraft. This is the reason why reference system *A* (parallel to *B)* is considered, as it will always be attached to the aircraft's nose. By considering a system parallel to system *B* (and, thus, to *A*) and fixed at a given component's CG, it is possible to determine the position of that component, relative to system *A*. Those parallel to body systems are referred as *Pb* , and can be seen in Fig. 3.

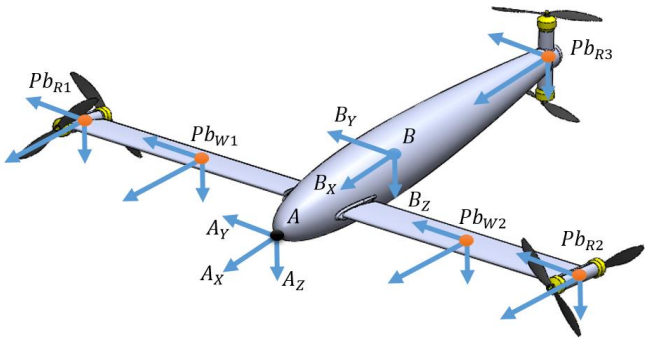

Fig. 3. Distribution of reference systems used in the model. Only the parallel to body reference system attached to the fuselage's CG is not shown.

In the case of the wings and their respective coaxial-rotors, the relative position of their respective *Pb* systems with respect to *A* is also a function of tilting angles ϕ_{E1} and ϕ_{E2} .

By knowing the coordinates of the relative position of all components with respect to *A* and their respective masses, it is possible to find the relative position of the aircraft's CG and its system *B* with (1). Where *m*, with its respective subscript, represents the mass of a given component and m_T represents the aircraft's total mass.

Now, knowing the coordinates of the relative position of a given component and from the aircraft's CG, both with respect to system *A*, a simple vectorial subtraction gives the relative position of that same component with respect to system *B*. As an example, for coaxial-rotor R_1 , with a tilting angle ϕ_{E1} , its position relative to *B* is given by (2).

$$\begin{bmatrix} X_{B_A} & Y_{B_A} & Z_{B_A} \end{bmatrix}^T = \frac{1}{m_T} \begin{bmatrix} X_{PbR1_A} & X_{PbR2_A} & X_{PbR3_A} & X_{PbW1_A} & X_{PbW2_A} & X_{F_A} \\ Y_{PbR1_A} & Y_{PbR2_A} & Y_{PbR3_A} & Y_{PbW1_A} & Y_{PbW2_A} & Y_{F_A} \\ Z_{PbR1_A} & Z_{PbR2_A} & Z_{PbR3_A} & Z_{PbW1_A} & Z_{PbW2_A} & Z_{F_A} \end{bmatrix} \begin{bmatrix} m_{R_1} \\ m_{R_2} \\ m_{R_3} \\ m_{W_1} \\ m_{W_2} \\ m_F \end{bmatrix} \quad (1)$$

$$\begin{bmatrix} X_{PbR1_B} \\ Y_{PbR1_B} \\ Z_{PbR1_B} \end{bmatrix} = \begin{bmatrix} X_{PbR1_A}(\phi_{E1}) \\ Y_{PbR1_A} \\ Z_{PbR1_A}(\phi_{E1}) \end{bmatrix} - \begin{bmatrix} X_{B_A} \\ Y_{B_A} \\ Z_{B_A} \end{bmatrix} \quad (2)$$

By knowing the coordinates of the relative position of a given component with respect to *B*, it is possible to transfer the inertial distribution, moments and forces produced by that component to the body-fixed system *B*. In addition, on the other way-around, aircraft's linear and rotational velocity vectors (originally defined relative to system *B*) can now be transferred to the respective component's *Pb* system. The drone's linear and rotational velocities may affect the behaviour of the component. As an example, considering again R_1 , (3) gives the relative wind-speed components acting on the coaxial-rotor, which affect its thrust and torque.

$$\begin{bmatrix} U_{R1} \\ V_{R1} \\ W_{R1} \end{bmatrix} = \left[Rot_Y(\phi_{E1}) \right]^{-1} \left\{ \begin{bmatrix} U \\ V \\ W \end{bmatrix} + \begin{bmatrix} P \\ Q \\ R \end{bmatrix} \times \begin{bmatrix} X_{PbR1_B} \\ Y_{PbR1_B} \\ Z_{PbR1_B} \end{bmatrix} \right\} \quad (3)$$

Where $Rot_Y(\phi_{E1})$ is a rotation matrix around the Y-axis, $\begin{bmatrix} U & V & W \end{bmatrix}^T$ is the linear velocity vector and $\begin{bmatrix} P & Q & R \end{bmatrix}^T$ is the angular velocity vector, both with respect to system *B*.

4. AIRCRAFT'S INERTIA

The products and moments of inertia of each component can be estimated with the use of a 3D modelling CAD software such as SolidWorks if the component's mass and dimensions are known. As an improvement of the conceptual design previously shown in Figs. 1 to 3, real items such as electronics, structural and other mechanical parts (like propellers) with their respective masses and dimensions were considered in order to obtain a realistic 3D model of the aircraft's wings, coaxial-rotors and fuselage. Fig. 4 shows the 3D rendered

SolidWorks' model, with an approximate total mass of 4,375 kg.

Fig. 4. Aircraft's 3D model in a symmetric configuration.

Knowing the coordinates of the relative position of each component with respect to *B* and through the Huygens-Steiner theorem of parallel axes, it is possible to transfer the moments and products of inertia of each component, to the coordinated body-fixed system *B.* Then, the overall inertia tensor J_T is given by the sum of the inertia tensor of every component.

$$J_T = J_{R1_B} + J_{R2_B} + J_{R3_B} + J_{W1_B} + J_{W2_B} + J_{F_B} \tag{4}$$

And taking the time derivative of (4), gives:

$$\dot{J}_T = \dot{J}_{R1_B} + \dot{J}_{R2_B} + \dot{J}_{R3_B} + \dot{J}_{W1_B} + \dot{J}_{W2_B} + \dot{J}_{F_B} \tag{5}$$

In this way, the aircraft's CG coordinates and the inertia tensor are functions of the tilting angles, while the time derivate of the aircraft's inertia tensor becomes a function of both the tilting angles and their time derivatives $\dot{\phi}_{Ei}$.

If the inertia tensor is to be considered as constant, and consequently its time derivative as null, the error between the model and the real aircraft would be enlarged.

To validate the calculation of the aircraft's inertia tensor, for a given value of its three tilting angles, the inertia tensor obtained by the equation model is compared with the inertia tensor obtained from the 3D model designed in the SolidWorks software.

Tables I and II show the aircraft's comparison of moments and products of inertia for different tilting angles.

TABLE I. Inertia tensor comparison for ϕ_{E1} = ϕ_{E2} = 15º and ϕ_{E3} = 90º, in a symmetrical configuration.

Moment/Product of Inertia [kg m²]	SolidWorks Model	Equation Model
Ixx	0.2680	0.2509
Ixy = Iyx	6.4269e-06	8.4972e-06
Ixz = Izx	0.0020	0.0032
Iyy	0.3782	0.3700
Iyz = Izy	-5.8999e-06	-4.6472e-06
Izz	0.6349	0.6124

TABLE II. Inertia tensor comparison for ϕ_{E1} = 120º, ϕ_{E2} = 45º and ϕ_{E3} = 65º, in a non-symmetrical configuration.

Moment/Product of Inertia [kg m²]	SolidWorks Model	Equation Model
Ixx	0.2694	0.2525
Ixy = Iyx	0.0014	0.0013
Ixz = Izx	0.0035	0.0030
Iyy	0.3797	0.3683
Iyz = Izy	-0.0003	-0.0002
Izz	0.6355	0.6083

5. EQUATIONS OF MOTION

The Newton-Euler equations of motion are used to describe the forces (6) and torques acting on the aircraft (7). By defining $v = [U \quad V \quad W]^T$ as the linear velocity vector and $w = [P \quad Q \quad R]^T$ as the angular velocity vector, both with respect to system *B*, then by Newton's second law applied to the body-fixed system:

$$m_T\left(\dot{v} + w \times v\right) = \sum F_B \tag{6}$$

$$J_T \cdot \dot{w} + \dot{J}_T \cdot w + w \times \left(J_T \cdot w\right) = \sum M_B \tag{7}$$

With $\times$ representing the cross product, $\sum F_B$ the sum of external forces and $\sum M_B$ the sum of external moments. It should be noticed that both the inertia tensor and its derivative are being considered. Additionally, it is considered that wings and coaxial-rotors will contribute for both forces and moments, while the fuselage contributes only for drag forces and the gravitational force will act upon the total aircraft's mass at its CG.

Gravitational Force

Defined in the inertial system *I*, gravitational force is transferred to the body-fixed system *B*, by the rotational matrix $R_{XYZ}|_I^B$, as function of the Euler angles ϕ (roll), θ (pitch) and ψ (yaw).

$$R_{XYZ}|_I^B = \begin{bmatrix} c\theta c\psi & s\psi c\theta & -s\theta \\ c\psi s\phi s\theta - c\phi s\psi & s\theta s\psi s\phi + c\phi c\psi & s\phi c\theta \\ c\psi c\phi s\theta + s\phi s\psi & c\phi s\psi s\theta - s\phi c\psi & c\theta c\phi \end{bmatrix} \tag{8}$$

$$F_{G_B} = R_{XYZ}|_I^B \cdot [0 \quad 0 \quad m_T g]^T \tag{9}$$

With *c* as cosine and *s* as sine functions and g as the gravity acceleration.

Fuselage Drag Force

Given by (10), fuselage drag force is already defined in system *B.* Air density is represented by ρ; The projected area normal

to each of the *B* system axes is represented by A_{Fi} and C_{DFi} the corresponding drag coefficient.

$$F_{DF_B} = -\frac{1}{2}\rho\begin{bmatrix} A_{FX}C_{DFX}U^2 & A_{FY}C_{DFY}V^2 & A_{FZ}C_{DFZ}W^2 \end{bmatrix}^T \quad (10)$$

Coaxial-Rotors' Thrust Forces and Moments

Equations (11) and (12) give the total thrust force and total torque for a given coaxial-rotor, respectively. The subscripts refer, respectively, to the upper hu and lower hl propellers of the coaxial-rotor.

$$T_{Ri} = T_{hu} + T_{hl} \quad (11)$$

$$Q_{Ri} = Q_{hu} - Q_{hl} \quad (12)$$

Moreover, for a given propeller its thrust force is considered as in (13) and its torque as in (14). Where Ct represents the propeller's thrust coefficient, Cq represents the propeller's torque coefficient, Ω its rotational speed and D its diameter.

$$T_h = \rho Ct \Omega^2 D^4 \quad (13)$$

$$Q_h = \rho Cq \Omega^2 D^5 \quad (14)$$

The coefficients Ct and Cq are found as polynomial equations which are function of the advance ratio J_{adr} of the propeller, given by (15), thanks to the experimental data provided by the manufacturers of the APC 10x3.8 SF propeller and the Scorpion M-3011-760KV brushless motor chosen for this project (which are used in all rotors). For a lower propeller, the effect of the induced wind speed from its corresponding upper propeller to it is also taken into account. U_{Ri} was given in (3).

$$J_{adr} = \frac{U_{Ri}}{\Omega D} \quad (15)$$

The thrust force of each coaxial-rotor is transferred to the *B* system, by its corresponding rotation matrix, as a function of the corresponding tilting angle ϕ_{Ei}. The total thrust force becomes the sum of the thrust forces of each coaxial-rotor.

$$F_{T_B} = Rot_Y(\phi_{E1})\begin{bmatrix} T_{R1} \\ 0 \\ 0 \end{bmatrix} + Rot_Y(\phi_{E2})\begin{bmatrix} T_{R2} \\ 0 \\ 0 \end{bmatrix} + Rot_X(\phi_{E3})\begin{bmatrix} 0 \\ T_{R3} \\ 0 \end{bmatrix} \quad (16)$$

Additionally, knowing the coordinates of each coaxial- rotor and its corresponding thrust forces, both with respect to *B*, the torque produced by the thrust forces is given by (17).

$$M_{T_B} = \begin{bmatrix} X_{PbR1_B} \\ Y_{PbR1_B} \\ Z_{PbR1_B} \end{bmatrix} \times F_{TR1_B} + \begin{bmatrix} X_{PbR2_B} \\ Y_{PbR2_B} \\ Z_{PbR2_B} \end{bmatrix} \times F_{TR2_B} + \begin{bmatrix} X_{PbR3_B} \\ Y_{PbR3_B} \\ Z_{PbR3_B} \end{bmatrix} \times F_{TR3_B} \quad (17)$$

Moreover, each coaxial-rotor contributes with two additional moments. The first one being the induced moment caused by the interaction of the air-flow passing through the propellers (18) and the second one being gyroscopic moment caused by the variation of the propeller's angular momentum.

$$M_{Q_B} = Rot_Y(\phi_{E1})\begin{bmatrix} Q_{R1} \\ 0 \\ 0 \end{bmatrix} + Rot_Y(\phi_{E2})\begin{bmatrix} Q_{R2} \\ 0 \\ 0 \end{bmatrix} + Rot_X(\phi_{E3})\begin{bmatrix} 0 \\ Q_{R3} \\ 0 \end{bmatrix} \quad (18)$$

For the gyroscopic moment, (19) gives the angular momentum of each coaxial-rotor, caused by the respective propellers' rotation, where I_h represents the propeller's inertia and $(\Omega_{hu} - \Omega_{hl})$ represents the rotation speed difference between upper and lower propellers. The total gyroscopic moment is then given by (20), where it becomes a function of upper and lower rotation speeds Ω_{hi}, accelerations $\dot{\Omega}_{hi}$, tilt angles ϕ_{Ei} and tilting speeds $\dot{\phi}_{Ei}$.

$$\begin{aligned} H_{R1_B} &= Rot_Y(\phi_{E1})\begin{bmatrix} I_h(\Omega_{hu} - \Omega_{hl}) & 0 & 0 \end{bmatrix}^T \\ H_{R2_B} &= Rot_Y(\phi_{E2})\begin{bmatrix} I_h(\Omega_{hu} - \Omega_{hl}) & 0 & 0 \end{bmatrix}^T \\ H_{R3_B} &= Rot_X(\phi_{E3})\begin{bmatrix} 0 & I_h(\Omega_{hu} - \Omega_{hl}) & 0 \end{bmatrix}^T \end{aligned} \quad (19)$$

$$M_{G_B} = \dot{H}_{R1_B} + w \times H_{R1_B} + \dot{H}_{R2_B} + w \times H_{R2_B} + \dot{H}_{R3_B} + w \times H_{R3_B} \quad (20)$$

The coaxial-rotor then becomes a system controlled by three inputs: tilt angle ϕ_{Ei}, upper propeller rotational speed Ω_{hu} and lower propeller rotational speed Ω_{hl}. However, based on the propeller's manufacturer data, a polynomial expression for the lower propeller rotational speed Ω_{hl} is found as a function of the upper propeller rotational speed Ω_{hu} and the coaxial-rotor relative wind-speed U_{Ri} in order to turn (12) close to zero for any given condition of propeller rotation or relative wind-speed. This allows the coaxial-rotors to turn (18) close to zero too. Hence, the coaxial-rotor is sufficiently controlled only by its tilt angle ϕ_{Ei} and its upper propeller rotational speed Ω_{hu}, as the corresponding lower propeller rotational speed Ω_{hl} follows the upper one. Fig, 5 shows this relation.

Wings' Aerodynamic Forces and Moments

Each wing is considered rectangular with a span of 0,5 m and a chord of 0,13 m, with no torsion angle, with a symmetrical aerodynamic profile and without ailerons or flaps. The chosen aerodynamic profile was the NACA0012.

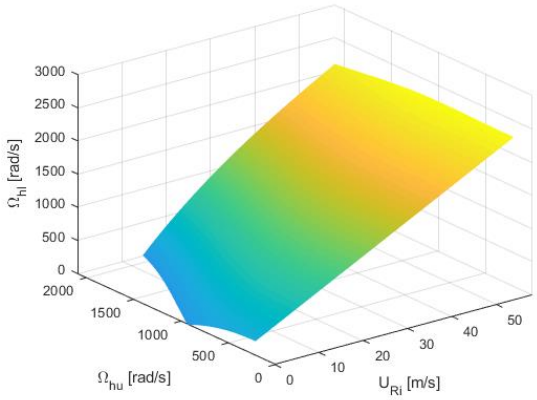

Fig. 5. Lower propeller rotational speed Ω_{hl} as a function of upper propeller rotational speed Ω_{hu} and coaxial-rotor relative wind-speed U_{Ri}, in order to diminish the coaxial-rotor's total induced torque.

Additionally, each wing is analyzed as two different sections, each one with its own angle of attack. Section 1 is closer to the wing's root and is free of the induced wing-speed effect of a coaxial-rotor's upper propeller. Section 2, closer to the wing's tip, is considered affected by the limited air "tube" formed by the upper rotor propeller, without radial compression of the flow and acting exclusively upon section 2 of a given wing, without altering the air flow of the adjacent section (Maqsood et al. 2010). The 'local' angle of attack of a given section in a wing is given by (21), where the subscript $WiSj$ refers to the 'i-th' wing and the 'j-th' section. The vertical $\left(W_{WiSj}\right)$ and horizontal $\left(U_{WiSj}\right)$ speed components, relative to the wing's section are obtained in (22), similarly as in (3), with the difference that for the wing's section, the relative speed components are "perceived" at the sections' aerodynamic center, at the mean aerodynamic chord, rather than at the wing's CG. The sections' aerodynamic center coordinates are found with a similar approach as the coordinates of the CG of a given component are found in (2).

$$\alpha_{WiSj} = \arctan\left(\frac{W_{WiSj}}{U_{WiSj}}\right) \tag{21}$$

$$\begin{bmatrix} U_{WiSj} \\ V_{WiSj} \\ W_{WiSj} \end{bmatrix} = \left[Rot_Y\left(\phi_{E1}\right)\right]^{-1} \left\{ \begin{bmatrix} U \\ V \\ W \end{bmatrix} + \begin{bmatrix} P \\ Q \\ R \end{bmatrix} \times \begin{bmatrix} X_{MAC_{WiSj_B}} \\ Y_{MAC_{WiSj_B}} \\ Z_{MAC_{WiSj_B}} \end{bmatrix} \right\} \tag{22}$$

The section's lift L_{WiSj} and drag D_{WiSj} forces are defined as (23) where A_{WiSj} refers to the section's area and C_L with C_D to the wing's lift and drag coefficients, respectively.

$$\begin{aligned} L_{WiSj} &= \frac{1}{2}\rho C_L A_{WiSj}\left(U_{WiSj}{}^2 + W_{WiSj}{}^2\right) \\ D_{WiSj} &= \frac{1}{2}\rho C_D A_{WiSj}\left(U_{WiSj}{}^2 + W_{WiSj}{}^2\right) \end{aligned} \tag{23}$$

The 2D version of the lift C_l and drag C_d coefficients are estimated for large angles of attack, based on the NACA0012 airfoil data. Then, the 3D version of these coefficients is obtained based on the approximation of the wing to an elliptical shape (optimal wing). Fig. 6 shows the estimation for the 2D coefficients, with the red dots as the experimental data and the blue lines as the estimated coefficients. Though a more refined method as Computational Fluid Dynamics analysis or wind-tunnel test is required to properly model the aerodynamic coefficients of the wings for large angles of attack, this initial estimation provides a basic understanding of the aerodynamic effects of the wing for the aircraft's model. It is worth noticing that the drag coefficient was limited to the value of 1.28, which is considered as the drag coefficient of a flat plate against the wind.

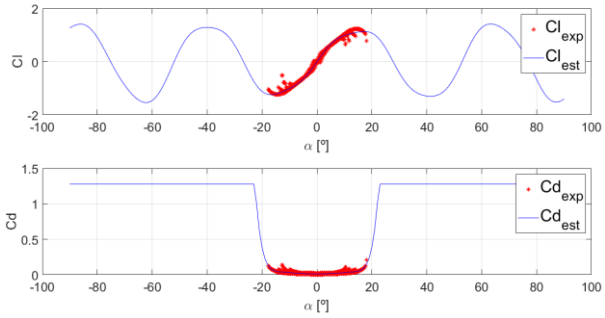

Fig. 6. 2D lift C_l and drag C_d coefficients. In red experimental data and in blue estimated curves.

Now the aerodynamic forces of a given wing's section can be transferred to the *B* system by a rotation of the sections' local angle of attack α_{WiSj} and then by a rotation of the wing's corresponding tilting angle ϕ_{Ei}. Equation (24) shows the aerodynamic forces for a given wing's section, with respect to system *B*. The total aerodynamic force is then the sum of the aerodynamic forces of all sections in both wings in (25).

$$F_{AWiSj_B} = Rot_Y\left(\phi_{Ei}\right)\left\{ Rot_Y\left(\alpha_{WiSj}\right) \begin{bmatrix} -D_{WiSj} \\ 0 \\ -L_{WiSj} \end{bmatrix} \right\} \tag{24}$$

$$F_{A_B} = F_{AW1S1_B} + F_{AW1S2_B} + F_{AW2S1_B} + F_{AW2S2_B} \tag{25}$$

Likewise, for a given wing's section, the aerodynamic moment caused by it is given by (26), with $M_{MAC_{WiSj_B}}$ as the 3D aerodynamic-profile moment estimated similarly as the lift and drag coefficients, as a function of the local angle of attack

α_{WiSj} . The total aerodynamic moment is then the sum of the aerodynamic moments of all sections in both wings in (27).

$$M_{AWiSj_B} = \begin{bmatrix} 0 \\ M_{MAC_{WiSj_B}} \\ 0 \end{bmatrix} + \begin{bmatrix} X_{MAC_{WiSj_B}} \\ Y_{MAC_{WiSj_B}} \\ Z_{MAC_{WiSj_B}} \end{bmatrix} \times F_{AWiSj_B} \quad (26)$$

$$M_{A_B} = M_{AW1S1_B} + M_{AW1S2_B} + M_{AW2S1_B} + M_{AW2S2_B} \quad (27)$$

Kinematic Relations

The dynamics of the system, defined in the body-fixed system *B*, must be transferred to the inertial system *I* to determine the aircraft's position and attitude in space.

The time derivative of Euler's angles (roll ϕ, pitch θ and yaw ψ) are related to the aircraft's rotational velocity, with respect to the body-fixed system with (28).

$$\begin{bmatrix} \dot{\phi} & \dot{\theta} & \dot{\psi} \end{bmatrix}^T = \begin{bmatrix} 1 & 0 & -\mathrm{s}\theta \\ 0 & \mathrm{c}\phi & \mathrm{s}\phi\mathrm{c}\theta \\ 0 & -\mathrm{s}\phi & \mathrm{c}\theta\mathrm{c}\phi \end{bmatrix}^{-1} \begin{bmatrix} P & Q & R \end{bmatrix}^T \quad (28)$$

The aircraft's linear velocity in space is related to its linear velocity with respect to the body fixed system by the inverse rotation matrix given in (8).

$$\begin{bmatrix} \dot{X}_I & \dot{Y}_I & \dot{Z}_I \end{bmatrix}^T = \left(R_{XYZ}\big|_I^B \right)^{-1} \begin{bmatrix} U & V & W \end{bmatrix}^T \quad (29)$$

By isolating $\dot{v}$ in (6) and $\dot{w}$ in (7), (30) and (31) are obtained:

$$\dot{v} = \begin{bmatrix} \dot{U} & \dot{V} & \dot{W} \end{bmatrix}^T = \frac{\sum F_B}{m_T} - w \times v \quad (30)$$

$$\dot{w} = \begin{bmatrix} \dot{P} & \dot{Q} & \dot{R} \end{bmatrix} = J_T^{-1} \left[\sum M_B - \dot{J}_T \cdot w - w \times \left(J_T \cdot w \right) \right] \quad (31)$$

From (28) to (31) it is possible to identify the non-linear system of the aircraft with its twelve states (*x*) and nine inputs (*u*):

$$x = \begin{bmatrix} X_I & Y_I & Z_I & U & V & W & \phi & \theta & \psi & P & Q & R \end{bmatrix}^T \quad (32)$$

$$u = \begin{bmatrix} \phi_{E1} & \phi_{E2} & \phi_{E3} & \Omega_{huR1} & \Omega_{hlR1} & \Omega_{huR2} & \Omega_{hlR2} & \Omega_{huR3} & \Omega_{hlR3} \end{bmatrix}^T \quad (33)$$

With inputs being three tilting angles ϕ_{Ei}, upper propellers' rotational speeds Ω_{hu} and lower propellers' rotational speeds Ω_{hl}. However, as discussed in Fig. 5, with lower propellers' rotational speeds Ω_{hl} following their corresponding upper ones, the control inputs become only six, rather than nine.

$$u = \begin{bmatrix} \phi_{E1} & \phi_{E2} & \phi_{E3} & \Omega_{huR1} & \Omega_{huR2} & \Omega_{huR3} \end{bmatrix}^T \quad (34)$$

6. SIMULATION AND CONTROL

With the non-linear model fully defined, it is necessary to test the model in a simulation environment in order to understand if the dynamics that were considered are in accordance with the physical principles and if the control variable inputs behave accordingly to effectively control the aircraft towards stabilization and the following of command references.

To test the aircraft's behaviour, the cruise or levelled flight is simulated. The drone starts with a constant forward speed *U* with all other state variables at zero, without linear or angular accelerations in any of its axes and its wings are tilted almost horizontally. For this flight condition, based on Allenspach et al. (2020) for optimal control, the Linear Quadratic Regulation technique with state feedback and integral action (LQRI) is chosen to control the linear velocity $\begin{bmatrix} U & V & W \end{bmatrix}^T$ and angular velocity $\begin{bmatrix} P & Q & R \end{bmatrix}^T$ state variables, with control input variables as defined by (34). The initial conditions of state and control variables are found in order to achieve the equilibrium point and then the system is linearized to obtain matrices A and B in (35). Additionally, it is assumed that all state variables are measurable.

$$\dot{x}_{6x1} = A_{6x6} x_{6x1} + B_{6x6} u_{6x1} \quad (35)$$

With cruise flight initial conditions defined by (36), Fig. 7 shows the response of state variables for 40 seconds of simulation in a Simulink environment. At t = 1s, a step input in the forward velocity *U* of 3 m/s is given until t = 10s. Then, from t = 20 s until t = 25 s, a negative step input of -5 º/s is given to the yaw variation *R*. Fig. 8 presents the corresponding variation of the input variables.

$$\begin{aligned} &U = 20\frac{m}{s}, \phi_{E1} = \phi_{E2} = 6,7^o, \phi_{E3} = 90^o, \\ &\Omega_{huR1} = \Omega_{huR2} = 794\frac{rad}{s}, \Omega_{huR3} = 723\frac{rad}{s}, \\ &\Omega_{hlR1} = \Omega_{hlR2} = 809\frac{rad}{s}, \Omega_{hlR3} = 771\frac{rad}{s} \end{aligned} \quad (36)$$

From the simulation results it can be seen that for the forward step acceleration *U*, as expected, both wings lean closer to zero while their respective coaxial-rotors accelerate and the rear coaxial-rotor maintains the 90º tilt while varying its acceleration in order to stabilize the vertical acceleration *W* and the pitch *Q* variation. Afterwards, with the yaw command *R* at t = 20 s, both wings rotate in opposite directions, having

the right wing leaned closer to zero and its right coaxial-rotor accelerating while the left coaxial-rotor deaccelerates. This produces a large amount of torque in the negative direction of the B_z axis (see fig. 3), which is expected for the aircraft in order to follow the commanded negative yaw turn. Meanwhile, the rear coaxial-rotor is tilted in order to produce a positive torque around the B_z axis and act as a "brake" in opposition to the right-coaxial rotor. It can be seen that all the while the control inputs variate in order for the drone to accompany the commanded inputs while preserving the stabilization of the aircraft.

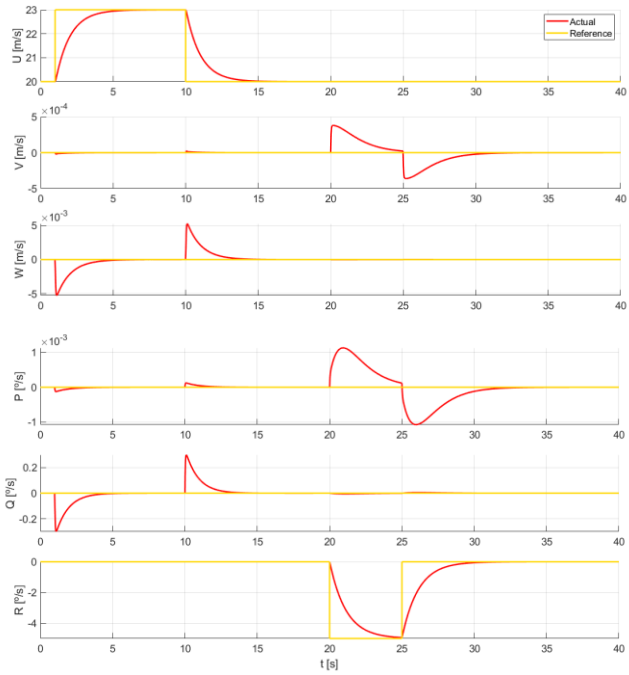

Fig. 7. State variable changes for step inputs in forward speed *U* and yaw speed *R*. In red the actual states and in yellow the references.

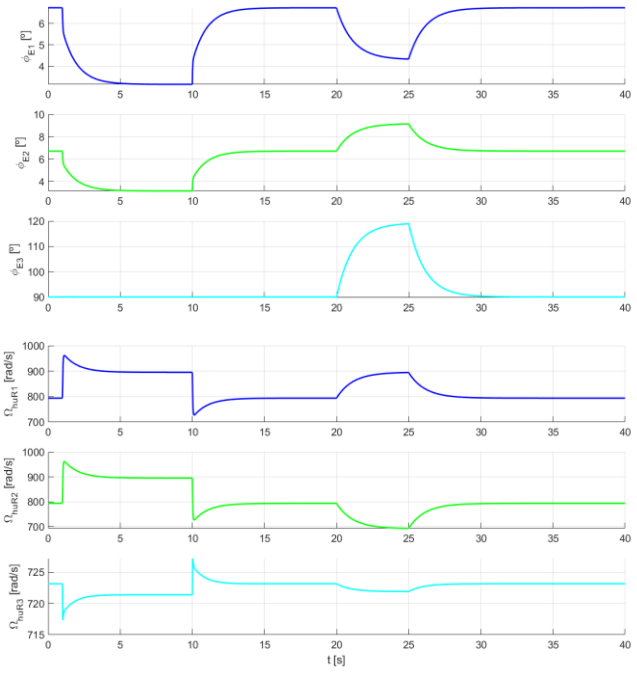

Fig. 8. Control input variable changes for step inputs in forward speed *U* and yaw speed *R*.

7. CONCLUSIONS AND FUTURE WORK

The proposed non-linear model of a novel VTOL tricopter drone that mixes the inclination of wings along with coaxial-rotors to generate lift and maneuver in the air was created and validated. The leveled-flight simulation with LQRI control in a Simulink environment demonstrated that the aircraft responds physically correct to given commands by varying the inclination of its wings and the acceleration of its coaxial-rotors. Future work will include testing and comparing other types of control techniques such as Adaptive control or with the aid of Artificial Neural Networks in order for the aircraft to follow trajectories and achieve transition between hover and cruise flight modes as proposed by Seonghun Yoon et al. (2014) and Autenrieb et al. (2019) for tilt-wing aircraft control.

REFERENCES

Alexis, K., Huerzeler, C. and Siegwart, R. (2013) "Hybrid modeling and control of a coaxial unmanned rotorcraftinteracting with its environment through contact", IEEE *International Conference on Robotics and Automation, ICRA'13*. Karlsruhe, Germany..

Allenspach, M., Bodie, K., Brunner M., Rinsoz, L., Taylor, Z., Kamel, M., Siegwart, R. and Nieto, J. (2020) "Design and optimal control of a tiltrotor micro aerial vehicle for efficient omnidirectional flight". *The International Journal of Robotics Research*, Vol. 39, Issue 10-11.

Autenrieb, J., Shin, H.S., Bacic, M. (2019) "Development of a Neural Network-based Adaptive Nonlinear Dynamic Inversion Controller for a Tilt-wing VTOL Aircraft" *International Workshop on Research, Education and Development on Unmanned Aerial Systems*. Cranfield, United Kingdom.

Bautista, A. J., Osorio, A., Lozano, R. (2017) "Modeling and Analysis of a Tricopter/Flying-Wing Convertible UAV with Tilt-Rotors", *International Conference on Unmanned Aircraft Systems, ICUAS'17,* Miami, Florida, United States.

Maqsood, A. and Go, T.H. (2010) "Optimization of hover-to-cruise transition maneuver using variable-incidence wing". *Journal of Aircraft*, Vol 47 (No.3).

Mikami, T., Uchiyama, K.. (2015) "Design of flight control system for quad tilt-wing UAV". *International Conference on Unmanned Aircraft Systems, ICUAS'15*, Denver, Colorado, United States.

Onen, A.S., Cevher, L., Senipek, M., Mutlu, T., Gungor, M., Uzunlar, I.O., Kurtulus, D.F. and Tekinalp, O. (2015) "Modeling and controller design of a VTOL UAV". *International Conference on Unmanned Aircraft Systems, ICUAS'15,* Denver, Colorado, United States.

Seonghun Yoon, Seungkeun Kim and Jinyoung Suk. (2014) "Neural Network Controller Design for a Single Tilt-wing UAV". *Asia-Pacific International Symposium on Aerospace Technology*, *APISAT*, Shanghai, China.

Zhong, L., Yuqing, H., Liying, Y., Jianda, H. (2016)"Control techniques of tilt rotor unmanned aerial vehicle systems: A review". *Chinese Journal of Aeronautics*, Vol. 28.